

Mechanical Comparison of Short Models of Nb₃Sn Low- β Quadrupole for the Hi-Lumi LHC

E. Takala, G. Ambrosio, N. Bourcey, L. Bianchi, D. W. Cheng, P. Ferracin, M. Guinchard, S. Izquierdo Bermudez, F. Mangiarotti, H. Pan, J.C. Perez, S. Prestemon, J. Ferradas Troitino, G. Vallone, C. Castro Sequeiro, S. Ferradas Troitino

Abstract—MQXF is the Nb₃Sn Low- β quadrupole magnet that the HL-LHC project is planning to install in the LHC interaction regions in 2026 to increase the LHC integrated luminosity. The magnet will be fabricated in two different lengths: 4.2 m for MQXFA, built in the US by the Accelerator Upgrade Project (AUP), and 7.15 m for MQXFB, fabricated by CERN. In order to qualify the magnet design and characterize its performance with different conductors, cable geometries and pre-load configurations, five short model magnets, called MQXFS, were fabricated, assembled and tested. We compare the mechanical behavior of short model magnets using experimental data and new numerical models that take into account the measured coil sizes as a function of position.

Index Terms—Superconducting magnets, Nb₃Sn wire, strain measurement, stress measurement, fiber bragg grating, optical fiber

I. INTRODUCTION

ONE of the main components of the high luminosity upgrade (HI-Lumi) [1] of the LHC (Large Hadron Collider) is the MQXF superconducting Nb₃Sn Low- β Quadrupole magnet [1]–[5]. The coils of MQXF need to be, azimuthally and axially, preloaded in order to counter the electro-magnetic forces. The azimuthal preload of MQXF relies on the so called bladder-key technology [6] in which water bladders are pressurized in the bladder slots (Fig. 1) in order to press the collars against the coils causing azimuthal compression. The loading keys are then inserted in their slots in order to sustain the azimuthal preload without the bladders that can then be removed. The axial loading relies on the four axial rods that are connected to plates compressing the coils at both ends. The rods are pretensioned by pulling them with the help of a piston and then fixing them in the plates with nuts. The axial and azimuthal strain is measured on the inner surface of the poles and at four different locations on the outer shell surface (Fig. 1). The strain in each location is converted to stress that is the measure of azimuthal preload. The axial strain is measured

This work was supported by the U.S. Department of Energy, Office of Science, Office of High Energy Physics, through the US LHC Accelerator Research Program (LARP) and the US LHC Accelerator Upgrade Project (AUP), and by the High Luminosity LHC project at CERN.

E. Takala, N. Bourcey, L. Bianchi, F. Salvador Ferradas Troitino, M. Guinchard, S. Izquierdo Bermudez, F. Mangiarotti, J.C. Perez, C. Castro Sequeiro are with CERN, CH-1211 Geneva 23, Switzerland (e-mail: eelis.takala@cern.ch)

G. Ambrosio is with Fermi National Accelerator Laboratory, Batavia, IL 60510 USA.

D. W. Cheng, P. Ferracin, H. Pan, S. Prestemon, G. Vallone, are with Lawrence Berkeley National Lab, Berkeley, CA 94720, USA

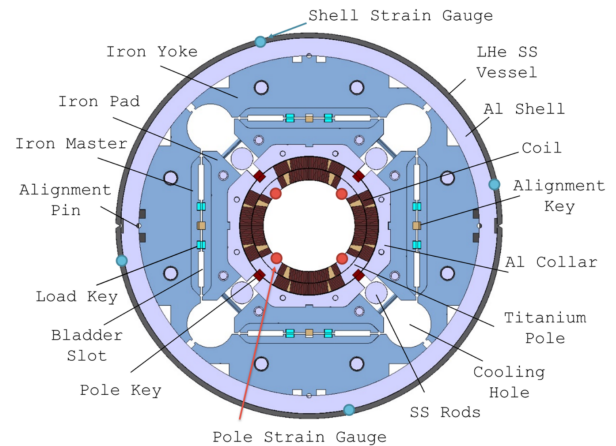


Fig. 1. The mechanical features of the MQXF magnet.

in each rod and converted to force that is the measure of axial preload. Imbalance is defined as the range of measured stress. The preload will further increase during the cool down due to the different thermal contraction between the support elements (shell, rods) and the rest of the structure.

The MQXF modeling and theory development has been done using octant ANSYS®-models [5], [7]–[11]. It is a great tool for fast computations and can provide a good understanding of the mechanical behavior of the magnet. However, the model cannot reproduce asymmetric behavior. In fact, the effect of pole stress variance measured on different quadrants within individual magnets was observed in the past. The stress variation of about ± 20 MPa was explained with azimuthal coil size variation using an analytic and the octant Finite Element Model (FEM) approach [10]. The coil size indeed varies being different along the length and among the coils. However, this is an asymmetric problem as the coils are joined together through mid-planes (MP) and the stress is shared between them. Moreover, the coil size varies also radially in an asymmetric way. In this paper we will present a full 2D FEM taking into account the measured coil sizes and we show that asymmetric coil sizes and local features there within can cause pole imbalance and asymmetric behavior. The latest short models of interest are MQXFS6, MQXFS6b, MQXFS6c and MQXFS6d that are assembled with coils produced using the PIT (Powder in Tube) conductor and equipped with optical Fiber Bragg Grating (FBG) strain sensors. We present the

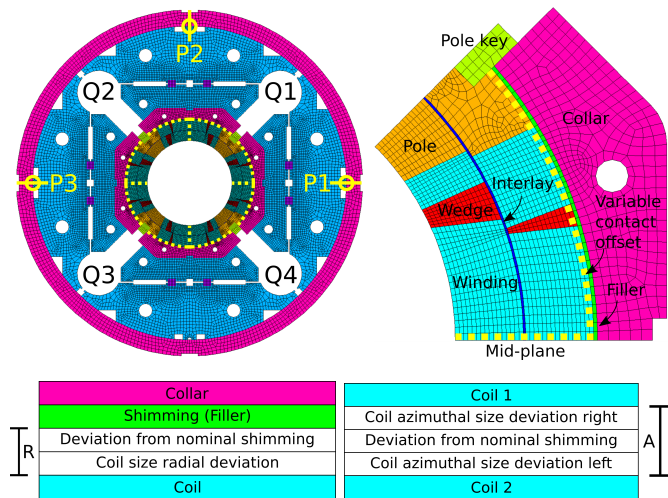


Fig. 2. The sketch of the full FEM is shown left on top: Q1...Q4 are the four quadrants. P1...P3 are points on the shell inner radius whose displacements are constrained in the azimuthal direction. The yellow dashed line represents a contact with variable offset. The sketch shown on top right is a close up view of Q1 first octant showing the environment of the coil and the collar. The sketches on bottom left and right are topological representations of the coil to collar (R) and mid-plane to mid-plane (A) contact offsets, respectively.

numerical and experimental results of cool down and powering as well as compare them with the previous magnets.

II. THE FE MODEL

The FEM shown in Fig. 2 is further developed from the octant model [8] that is copied via rotation to the four quadrants (Q1...Q4). The resulting octants are mirrored and merged together in order to get the full geometry. The constraints at points P1...P3 need to be defined in order to fix the model in place without constraining any two points relative to one another. In the global context, there are three degrees of freedom: 1. vertical movement, 2. horizontal movement and 3. rotation. The first and third are constrained at P1 and P3, the second at P2. Any additional constraint would lead to an overconstrained model. For example, imagine bringing P1 and P2 to the same location in a model where all the parts except the shell are infinitely rigid. The points would meet at the only allowed common location that is the origin, thus pushing the model (and P3) further left and rotating the model clock-wise. Note, there is no reaction at P3 that simply determines the unique orientation of the model. Now, let us consider adding an azimuthal constraint to P4 (symmetric about the origin with P2). The solution w.r.t. P3 and P4 would have to be symmetric and thus the clock-wise rotation would be canceled due to the symmetric reactions at P3 and P4. The emergence of these reactions show that the model would be overconstrained.

The coil sizes are added to the coil-collar interface and the MP-MP interfaces varying the contact element offset (gap or interference) as a function of position. The coil-collar contact offset takes into account the shape of the coil and the radial shimming (nominal shimming plan shown in [11]). The MP-MP contact takes into account the coil shape on both sides and the MP shims. In [11] it was noted that the coil pack size determined in the TF-KP (transfer function - key plot)

analysis yielded on average 100 μm lower value than the value calculated according to the shimming plan. There are two possibilities: 1. the coil is smaller than measured, thus additional 100 μm can be reduced from the coil-collar contact offset, or 2. the structure does not exactly match their design values and thus one can add 100 μm to the loading key size. The first option fits slightly better in the case of MQXFS6b that was the first magnet under investigation and was thus chosen as the standard procedure. The coil is given isotropic bi-linear material model with modulus and tangent modulus of 20 GPa and 40 GPa, respectively, and yield stress of 1 MPa. Thus, the coil has a modulus of 20 GPa during the preload and 40 GPa during the powering (when the pole unloads [12]). Note that in [8] the respective approximate values from ten stack measurements are 14 GPa and 27 GPa. However, the chosen values fit better with the experimental strain gauge data.

III. COIL SIZE ASYMMETRY

Fig. 3 shows the coil sizes for MQXFS3a/3b/3c/4/5/6/6b/6c/6d measured with FaroArm® before each coil pack assembly. Note that LP7 and LP8 were developed and produced in an earlier R&D program called LARP [13]. The measured data is aligned radially to the outer surface of the coil and azimuthally to the pole key slot [14].

MQXFS6b/c/d inherited their coils from MQXFS5/S6 and so did MQXFS3c inherit from MQXFS3a/b. The shapes of these reassembled coils are slightly different from the virgin coils (Fig. 3). Thus they deform plastically when tested. The resulting shape resembles the so called dent in [11]; the radius is reduced near the MP whereas the opposite is true near the poles. According to FEM the coils take a similar shape when preloaded. Compare for example in Fig. 4 the highest/lowest preload (MQXFS3c/6c, respectively).

The MP excess is often asymmetric (different on right and left MP of the coil) and the shape has a sharp feature in the middle. The asymmetric excess can misalign the coil as it is compensated with symmetric MP shimming [11] (for example one sided pole key contact of Q2 and Q4 in MQXFS6 in Fig. 4). In principle, asymmetric MP shimming could be used to conform the alignment. The sharp feature can cause local stress intensification in the MP that is under high stress during the powering (see for example MQXFS3 MP Q1 to Q2). However, the composition of this feature is unknown and it is possible that the FEM overestimates its effect.

IV. POLE IMBALANCE

The azimuthal room temperature preload, cool down and pole unloading of all the short models is simulated with the FEM and compared with the experimental results. Due to the excellent performance of MQXFS4, reaching the ultimate in only 6 training quenches, it became the reference magnet in terms of preload targets. Interestingly, it also has the largest pole imbalance and is thus chosen as the example. In the next section a summary of all the results is presented. Fig. 5 shows a mechanical signature of MQXFS4 with FEM predictions. The signature contains the refined TF-KP analysis and the pole unloading curve. Note that the last point is of the cool

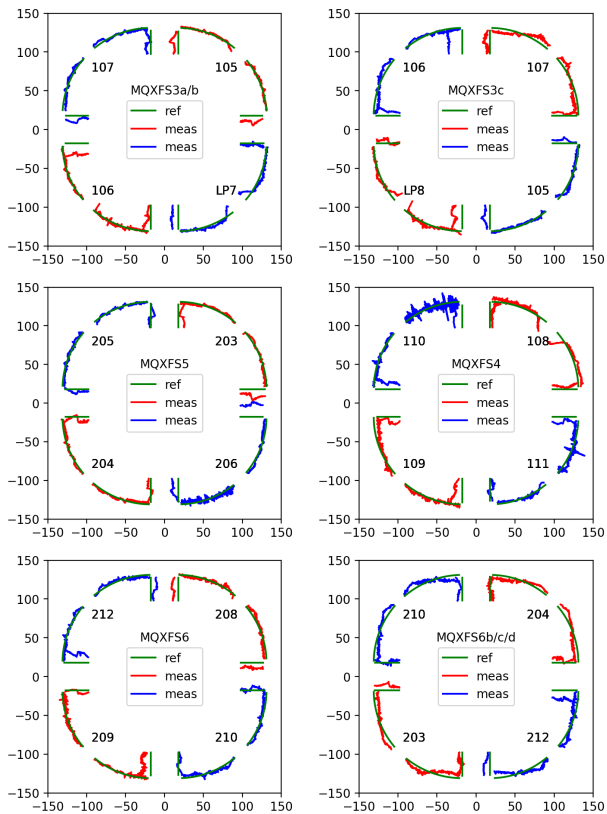


Fig. 3. Coil sizes in the cross-section at the center of the magnet. The scale is in mm, however, the deviation of measured and reference values are scaled with a factor of 100 (1 unit=10 μ m).

down that is estimated from the pole unloading (both FEM and measured). The azimuthal preload at cold measured directly on the pole sometimes suffers from an offset. Thus, a more reliable convention is developed that is based on the change of azimuthal stress during the powering $\Delta\sigma_\theta$ (this is called pole unloading). The prestress is defined as 10 MPa – $\max \Delta\sigma_\theta$ (some tension is allowed on the pole) [12].

The FEM predicts a shift below the no pole key line in TF and a high pole imbalance (highest compression in coil 108). Pole key/no pole key means that the collars are/are not in contact with the pole keys [8], respectively (Fig. 1). According to the FEM MQXFS4 has one sided late pole key contacts at key size 13.6 mm (Q2) and 13.85 mm (Q3) and late pole key contacts at cold (all, Fig. 4). Note that the one sided contacts do not have an effect on the TF nor on the KPs (Fig. 5).

The FEM shell KP is in very good agreement with the measurements whereas there is a pole contact key shift of about 100 μ m compared to the FEM prediction. Contact key is the theoretical loading key that enforces a contact between the structure and the coil pack before inducing any stress. If a line is fitted through the linear region of the KP, the contact key size can be estimated to be at the intersection of the key size axis and the line [11].

The FEM predicts a pole imbalance of 20 MPa at unloading, measurements show 41 MPa. Note in Fig. 5 pole unloading that the order of coils in terms of stress is predicted correctly (same color means same coil). The largest stress is in coil

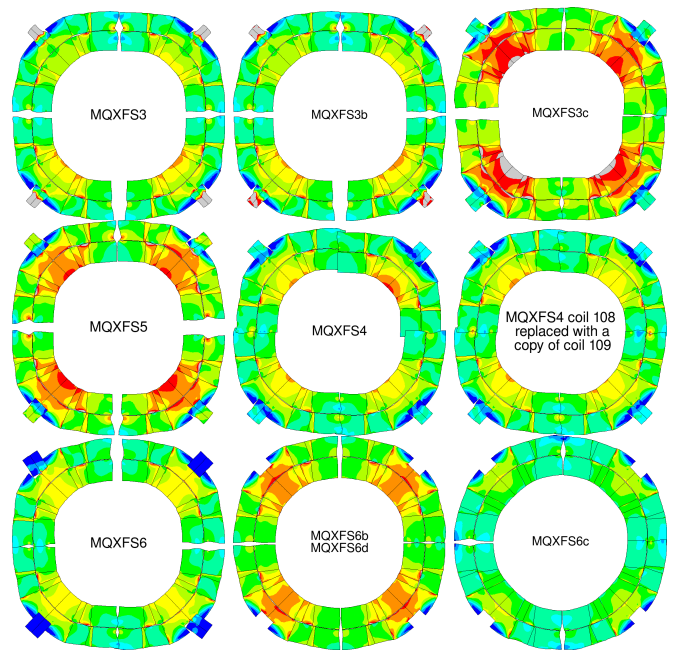


Fig. 4. The Von Mises stress in coil cross-section after cool down according to the FEM. The minimum and maximum values of compression are represented by blue and red colors (0 MPa and 150 MPa), respectively. The displacement is scaled by a factor of 50. Note that the imaginary magnet MQXFS4 with coil 108 replaced with a virtual copy of coil 109 also assumes the correct mid-plane shimming, *i. e.* shimming of that coil, to have the most equal mid-plane excess between the coils.

108 that has a rare indentation near the pole key slot (Fig. 3). Similar features are in coils LP7 and LP8 that also lead to high pole imbalance and high pole compression in that particular coil. These observations are made in both the FEM and the measurements. According to FEM the indentation enforces pole bending that increases pole compression (resembles the MP bump effect in [11]). In fact, when coil 108 (Q1) is replaced with a virtual copy of coil 109 (Q3) in FEM, the predicted imbalance drops from 20 MPa down to 7.5 MPa with the lowest stress in Q1 (see Fig. 4).

V. MAGNET COMPARISON

Fig. 6 (earlier plots and their analysis can be found in [9], [10]) and Table I show that most of the magnets have been preloaded to nominal conditions in terms of countering the electro-magnetic forces. The nominal azimuthal and axial preloads for MQXF are 120 MPa and 1.2 MN, respectively. The exceptions are MQXFS3, MQXFS3c and MQXFS6c, with low axial, high azimuthal and low azimuthal preloads, respectively. Those with nominal azimuthal preload do not all have the same shell stress due to pole key influence that can reduce the stress transfer from shell to coils [8]–[10]. The shell imbalance is mostly less than 25 MPa, except in MQXFS6b (the top gauge has considerably lower value compared to the others for an unknown reason). The FEMs show 0 MPa - 2 MPa shell imbalance values. It is possible that the instrumentation and the local conditions near the sensors have a role in this uncertainty.

In general the pole unloading depends mainly on the azimuthal preload of the pole. Neither the axial preload nor the

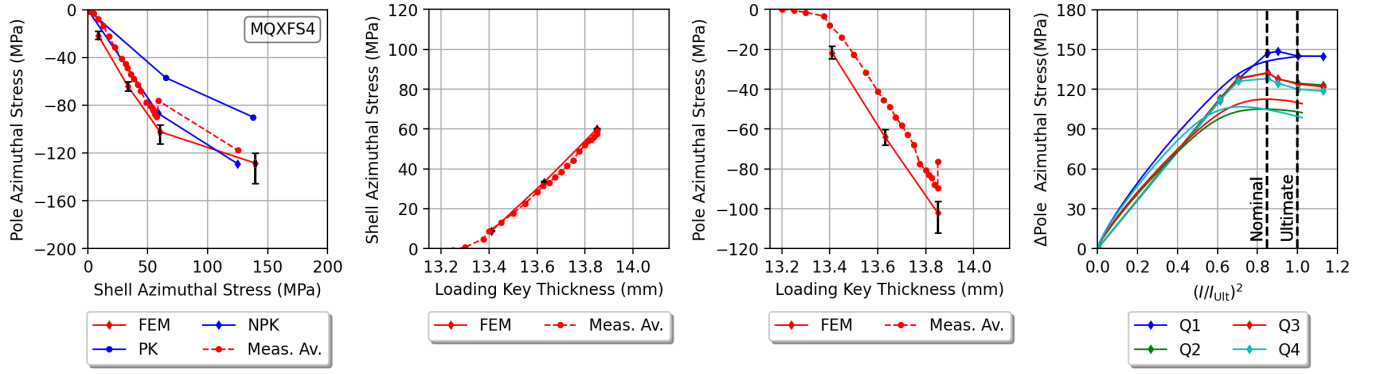


Fig. 5. The mechanical signature of MQXFS4 short model compared with the FEM predictions. Starting from left: Transfer function (TF), shell key plot (shell KP), pole key plot (pole KP), pole azimuthal vs current squared (pole unloading). The PK and NPK mean pole key and no pole key lines in the TF. Red diamonds with solid lines represent the FEM prediction, red circles with dashed lines represent the measured average in TF and KPs. The black error bars represent the highest and lowest stress values of the four quadrants according to FEM. The blue, green red and cyan solid lines represent quadrants 1, 2, 3 and 4, respectively, in the last column. The lines with diamonds and corresponding colors represent the FEM predictions.

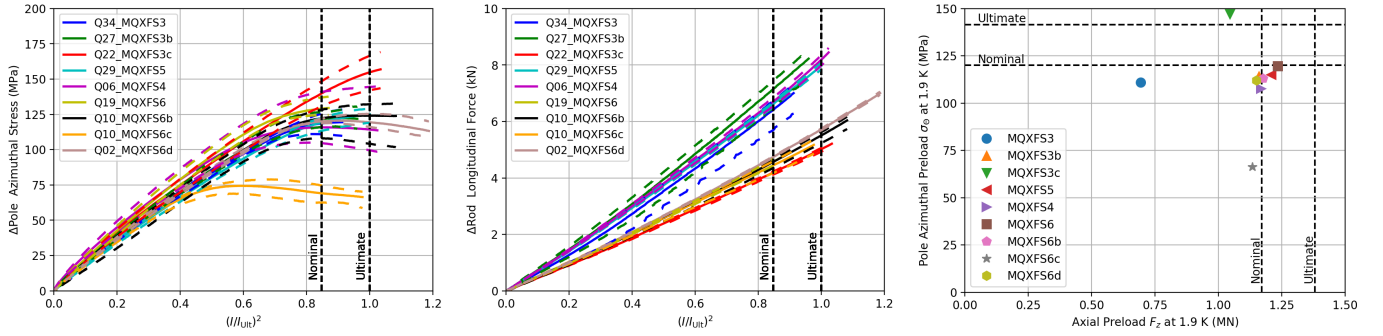


Fig. 6. A summary of pole unload, change of rod force during powering and summary plot of MQXF short model preload values at cold. The Q-number in the legend represents the training quench order number whose data is used in the plot and also in determining the preload values in the summary plot. Note that quality is one criteria for choosing the data and thus it is not necessarily of the highest quench. The dashed lines represent the minimum/maximum. Note that axial preload (also axial force) is the sum of the rod forces.

TABLE I

A COMPARISON OF COOL DOWN DOWN VALUES IN MQXFS MAGNETS. THE SLOPES ARE FITTED UNTIL 80% OF THE MAXIMUM STRESS/FORCE.

Magnet	MQXFS3		MQXFS3b		MQXFS3c		MQXFS5		MQXFS4		MQXFS6		MQXFS6b		MQXFS6c		MQXFS6d	
Value type	Meas.	FEM	Meas.	FEM	Meas.	FEM	Meas.	FEM	Meas.	FEM	Meas.	FEM	Meas.	FEM	Meas.	FEM	Meas.	FEM
Shell stress (MPa)	174	196	166	187	156	190	181	191	121	140	112	123	128	149	82	100	119	149
Shell imbalance (MPa)	9	2	9	2	25	1	4	2	6	2	20	1	53	0	25	0	28	0
Pole stress (MPa)	-111	-123	-114	-124	-147	-166	-115	-151	-108	-125	-120	-116	-113	-132	-66	-73	-112	-132
Pole imbalance (MPa)	18	24	15	25	26	33	10	5	41	20	13	3	27	3	6	4	7	3
Pole slope (MPa)	168	187	170	187	180	182	159	183	188	183	192	191	168	185	174	184	168	185
Slope imbalance (MPa)	3	6	19	5	20	2	8	1	25	3	21	1	29	1	10	1	11	1
Axial force (MN)	0.69		1.16		1.05		1.21		1.17		1.23		1.18		1.13		1.15	
Rod imbalance (kN)	11.87		10.92		7.39		14.08		8.52		7.39		2.99		3.97		1.19	
Rod slope (kN)	7.6		7.57		5.04		7.92		8.19		5.54		5.61		5.36		5.84	

influence of pole key has a strong effect on the unloading behavior. The pole unload slope is 175 MPa with an imbalance of 11% on average. The lowest and highest slopes among all the coils are 150 MPa (coil 203 in MQXFS6b) and 204 MPa (coil 210 in MQXFS6).

The pole imbalance is typically around 10 MPa - 25 MPa. In MQXFS4 the imbalance is 41 MPa that according to the FEM is explained by the indentation on the pole surface. Similar indentation features are in MQXFS3/S3b/S3c magnets that are also predicted having a large pole imbalance. This is the case according to the pole unloading (see MQXFS3/S3b/S3c/S4 vs MQXFS5/S6/S6b/S6c/S6d). However, MQXFS6b is an ex-

ception due to the unexplained behavior of coil 203, although, it is possibly explained by an instrumentation issue as the strain sensor wasn't functional anymore in MQXFS6d.

The axial force is mostly at nominal conditions except in MQXFS3 where it is 0.69 MN. The rod imbalance is 3% on the average. The two different slopes of rod force (5.4 kN and 7.8 kN) during powering can be categorized based on the two different mechanical structures [11]. In [9] it is proposed that this could be due to the different modulus of thin and thick iron laminates or a different coil-collar friction coefficient. MQXFS6c is the same as MQXFS6b but after the warm up it was unloaded, azimuthally, from 13.85 mm down

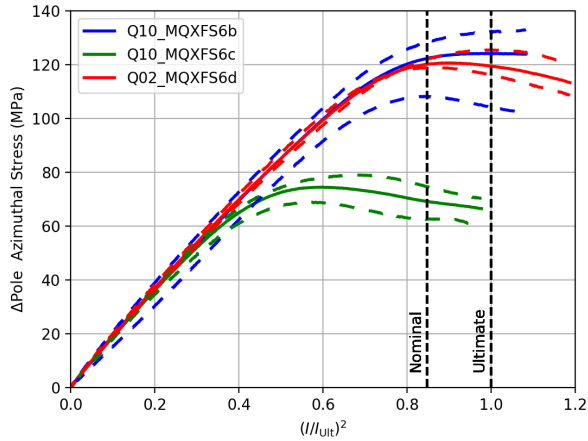


Fig. 7. A comparison of MQXFS6b/S6c/S6d pole unloading. See Fig. 6 for explanation of notations. Note that the coils of these magnets were measured with optical FBG strain sensors.

to 13.6 mm in terms of key size and MQXFS6d is again the same but loaded back with the MQXFS6b setup. The effect of the azimuthal unload to rod axial force based on the 3D octant FEM [7] is -55 kN, which is very close to the measured change from MQXFS6b to MQXFS6c (-42 kN). Loading back to the virgin setup the change from MQXFS6c to MQXFS6d is only 17 kN. However, in MQXFS6d only 2 rod gauges were functional, which could explain the difference and the low rod imbalance (Table I).

VI. THE EFFECT OF AZIMUTHAL PRELOAD

Despite the many differences, all but one of the magnets reached the nominal current that shows the robustness of the MQXF design [15], [16]. MQXFS6 is the exception that was limited by coil 208 inner pole turn [17]. However, MQXFS6b with a similar mechanical setup, two coils replaced and without pole key reached the record highest field gradient, surpassing the ultimate current with 93% of the short sample limit at 1.9 K and reached nominal with zero and ultimate current with one training quench [18]. MQXFS6b, MQXFS6c and MQXFS6d are the same magnet assembly loaded consecutively up to 113 MPa, reduced to 66 MPa and increased to 112 MPa azimuthal preloads, respectively. The difference is highlighted in Fig. 7 pole unloading plot. It is interesting to observe that the length of training in these magnets was zero, 12 and zero quenches, respectively [18]. This shows that reducing the azimuthal preload that increases coil movement increases the training length to ultimate in MQXF. At the time of writing, MQXFS6d has outperformed all of the previous magnets reaching more than 95% of the short sample limit at 1.9K and 98 % at 4.5K. Note that MQXFS6b, MQXFS6c and MQXFS6d have, mechanically, the most symmetric coil pairing configuration of all the magnets according to the FEM (Fig. 4).

VII. CONCLUSION

MQXF is a robust design that can successfully support its coils with different global and local preload conditions. The

short model magnet series has been continued with four new magnets, namely MQXFS6/S6b/S6c/S6d, using the PIT conductor and equipped with optical strain sensors. Mechanically, MQXFS6/S6b/S6d are targeted to the MQXFS4 preload that enabled the fastest virgin magnet training with preload close to nominal. Interestingly, MQXFS4 features an indentation in the pole of coil 108 that causes pole compression and large pole imbalance. This effect has been reproduced with a full 2D FEM using real coil sizes at the coil to collar and MP to MP interfaces and explained as a mid-plane bump - like bending effect. Furthermore, coil 108 was replaced in the FEM with a copy of coil 109 that doesn't have the feature; the coil imbalance dropped from 20 MPa to 7.5 MPa. MQXFS3/S3b/S3c were assembled with coils LP7 and LP8 that also feature the same pole indentation leading to similar pole imbalance according to the model. Indeed, pole unloading analysis supports this prediction showing the highest compression in that coil with the pole indentation.

Some of the coils presented here have been used in more than one assembly. A shape comparison of virgin and tested coils suggest that the coils are irreversibly deformed to a shape similar to that of a coil under preload according to FEM. The predictions of the full 2D model on preload characterization are in a fairly good agreement with the measurements. Generally, the shell is in an excellent agreement whereas in the pole there is more uncertainty that manifests itself mainly in the contact key shift. Moreover, throughout the magnets there is an unknown 100 μm shell contact key discrepancy that calls either for the radial shimming reduction or the loading key shift in the FEM depending on the source of the discrepancy. The new results favor slightly that the source is in the structure, however the difference of the two methods is just 20 μm in contact key size.

In the light of the new model, MQXFS6/S6b/S6c/S6d magnets are fairly well understood no pole key cases. Moreover, MQXFS6c/S6d are merely MQXFS6b with azimuthal unloading from 113 MPa to 66 MPa (-47 MPa) and loading up to 112 MPa in terms of pole compression, respectively. The axial loading setup was not changed, however the effect from MQXFS6b to MQXFS6c via Poisson's effect is 1.18 MN to 1.13 MN (-42 kN). In MQXFS6b cool down, the small pole imbalance of 3 MPa predicted by the model is ruined by coil 203 that deviates roughly 30 MPa from the others, which could be an artifact due to instrumentation. In MQXFS6c the imbalance (6 MPa) is more along the lines of the prediction (4 MPa). MQXFS6b/S6c/S6d have the most symmetric coil pairing configuration of all the magnets according to the FEM.

The powering tests of MQXFS6b/S6c/S6d show that lowering the azimuthal prestress lowers the critical current of the magnet and increases the length of training in MQXF that could be explained by increased coil motion during the ramp-up.

VIII. ACKNOWLEDGEMENTS

The authors thank the colleagues in the 927 laboratory and SM18 test facility for manufacturing and testing.

REFERENCES

- [1] G. Apollinari, I. B. Alonso *et al.*, “High-Luminosity Large Hadron Collider (HL-LHC) - Preliminary Design Report,” Tech. Rep., eds., Geneva, Switzerland: World Scientific, Dec. 2015.
- [2] E. Todesco, H. Allain *et al.*, “Design Studies for the Low-Beta Quadrupoles for the LHC Luminosity Upgrade,” *IEEE Transactions on Applied Superconductivity*, vol. 23, no. 3, pp. 4 002 405–4 002 405, 2013.
- [3] E. Todesco, H. Allain *et al.*, “A First Baseline for the Magnets in the High Luminosity LHC Insertion Regions,” *IEEE Transactions on Applied Superconductivity*, vol. 24, no. 3, pp. 1–5, 2014.
- [4] P. Ferracin, G. Ambrosio *et al.*, “Magnet Design of the 150 mm Aperture Low- β Quadrupoles for the High Luminosity LHC,” *IEEE Transactions on Applied Superconductivity*, vol. 24, no. 3, pp. 1–6, 2014.
- [5] P. Ferracin, G. Ambrosio *et al.*, “Development of MQXF: The Nb₃Sn Low- β Quadrupole for the HiLumi LHC,” *IEEE Transactions on Applied Superconductivity*, vol. 26, no. 4, pp. 1–7, 2016.
- [6] S. Caspi, S. Gourlay *et al.*, “The use of pressurized bladders for stress control of superconducting magnets,” *IEEE Transactions on Applied Superconductivity*, vol. 11, no. 1, pp. 2272–2275, 2001.
- [7] M. Juchno, G. Ambrosio *et al.*, “Mechanical Qualification of the Support Structure for MQXF, the Nb₃Sn Low- β Quadrupole for the High Luminosity LHC,” *IEEE Transactions on Applied Superconductivity*, vol. 26, no. 4, pp. 1–6, 2016.
- [8] G. Vallone, G. Ambrosio *et al.*, “Mechanical Performance of Short Models for MQXF, the Nb₃Sn Low- β Quadrupole for the Hi-Lumi LHC,” *IEEE Transactions on Applied Superconductivity*, vol. 27, no. 4, pp. 1–6, 2017.
- [9] G. Vallone, G. Ambrosio *et al.*, “Mechanical Analysis of the Short Model Magnets for the Nb₃Sn Low- β Quadrupole MQXF,” *IEEE Transactions on Applied Superconductivity*, vol. 28, no. 3, pp. 1–6, 2018.
- [10] G. Vallone, G. Ambrosio *et al.*, “Summary of the Mechanical Performances of the 1.5 m Long Models of the Nb₃Sn Low- β Quadrupole MQXF,” *IEEE Transactions on Applied Superconductivity*, vol. 29, no. 5, pp. 1–5, 2019.
- [11] E. Takala, G. Ambrosio *et al.*, “Preload Characterization of Short Models of MQXF the Nb₃Sn Low- β Quadrupole for the Hi-Lumi LHC,” *IEEE Transactions on Applied Superconductivity*, vol. 30, no. 4, pp. 1–6, 2020.
- [12] G. Vallone and P. Ferracin, “Modeling Coil-Pole Debonding in Nb₃Sn Superconducting Magnets for Particle Accelerators,” *IEEE Transactions on Applied Superconductivity*, vol. 27, no. 8, pp. 1–11, 2017.
- [13] S. A. Gourlay, G. Ambrosio *et al.*, “Magnet R&D for the US LHC Accelerator Research Program (LARP),” *IEEE Transactions on Applied Superconductivity*, vol. 16, no. 2, pp. 324–327, 2006.
- [14] J. Ferradas Troitino, P. Bestmann *et al.*, “Applied Metrology in the Production of Superconducting Model Magnets for Particle Accelerators,” *IEEE Transactions on Applied Superconductivity*, vol. 28, no. 3, pp. 1–6, 2018.
- [15] F. Mangiarotti, H. Bajas *et al.*, “Test Results of the CERN HL-LHC Low- β Quadrupole Short Models MQXFS3c and MQXFS4,” *IEEE Transactions on Applied Superconductivity*, vol. 29, no. 5, pp. 1–5, 2019.
- [16] H. Bajas, G. Ambrosio *et al.*, “Test Result of the Short Models MQXFS3 and MQXFS5 for the HL-LHC Upgrade,” *IEEE Transactions on Applied Superconductivity*, vol. 28, no. 3, pp. 1–6, 2018.
- [17] F. J. Mangiarotti, G. Willering *et al.*, “MQXFS56 short model test results,” Tech. Rep., eDMS - 2144878, CERN.
- [18] F. Mangiarotti, M. Duda *et al.*, “Powering performance and endurance beyond design limits of HL-LHC Low-Beta Quadrupole Magnets Models,” *IEEE Transactions on Applied Superconductivity*, 2020, submitted.